Brachyury expression levels predict lineage potential and axis-forming ability of *in vitro* derived neuromesodermal progenitors

running title: Brachyury dictates neuromesodermal lineage specification

Anahí Binagui-Casas*[1], Anna Granés*[1], Alberto Ceccarelli[2], Eleni Karagianni[3], Daniel Lopez Ramajo[1], Rosa Portero[1], Matthew French[4], Jen Annoh[1], Frederick C.K. Wong[5], Sally Lowell[1], Osvaldo Chara[2,6], Valerie Wilson[1]

1. Institute for Regeneration and Repair, Institute for Stem Cell Research, School of Biological Sciences, University of Edinburgh, 5 Little France Drive, Edinburgh EH16 4UU, Scotland
2. School of Biosciences, University of Nottingham, Sutton Bonington Campus, Nottingham LE12, UK
3. GSK, Hills Rd, Cambridge CB2 0QQ, UK
4. Department of Genetics, University of Cambridge, Cambridge, CB2 3EH UK,
5. The Wellcome Sanger Institute, Wellcome Genome Campus, Cambridge CB10 1SA, UK
6. Instituto de Tecnología, Universidad Argentina de la Empresa, Buenos Aires, Argentina.

* joint first authors

co-corresponding authors: a.binagui-casas@ed.ac.uk, v.wilson@ed.ac.uk

Keywords: Neuromesodermal progenitors, Axis elongation, Pluripotent stem cells, Mesoderm, Neurectoderm, In vitro differentiation, Single cell

Abstract

Neuromesodermal progenitors (NMPs) produce the spinal cord and musculoskeleton in the elongating anterior-posterior axis. *In vivo*, NMPs possess dual potency, coinciding with regions coexpressing SOX2 and TBXT. *In vitro*, SOX2$^+$TBXT$^+$ cells can be produced from pluripotent cells and, like their *in vivo* counterparts, colonise neural and mesodermal embryonic regions. However, the potency of individual *in vitro* SOX2$^+$TBXT$^+$ cells is unclear, confounding comparisons with *in vivo* data. To address this, we developed a dual *Sox2/Tbxt* reporter mouse ESC line and demonstrate that single *in vitro* derived *Sox2/Tbxt*-expressing cells are bipotent NMPs. *In vitro* derived NMPs also exhibit lateral plate mesoderm potency when cultured in inductive conditions. Surprisingly, we identified two successively higher *Tbxt* threshold expression levels that correspond to mesoderm bias and specification, respectively. Moreover, clonally plated Sox2$^+$/Tbxt$^+$ cells self-propagate. Media and substrate composition alter the specification thresholds and consequent differentiation outcomes of *in vitro* derived mouse NMPs. Using this live reporter line, we uncover rapid inhibition of axis elongation following TBXT downregulation in response to WNT or NOTCH inhibition. In summary, this tractable cell line provides evidence supporting a key role for TBXT in tuning cell fate to drive axis elongation.

36 **Introduction**

37 In vertebrates, the head-to-tail (or anteroposterior, AP) body axis forms during early embryonic
38 development. In mice, where this process is well characterised (Wymeersch et al., 2021), a transient
39 population of progenitors, collectively called neuromesodermal competent cells (NMCs), produces
40 both paraxial mesoderm and neurectoderm as the AP axis elongates in post-gastrulation stages. NMC
41 populations across vertebrates harbour cells with functional heterogeneity, including bona fide
42 neuromesodermal progenitors (NMPs) (Binagui-Casas et al., 2021). Fate mapping has shown that
43 neuromesodermal potency is found at the posterior end of various vertebrate embryo species and
44 this region coincides with the co-expression of the transcription factors SOX2 and Brachyury (TBXT)
45 (Wymeersch et al., 2021). Importantly, the hallmark of NMPs is their developmental potential to
46 generate both neuroectodermal and mesodermal lineages, two separate germ layers, at post-
47 gastrulation stages (Guillot et al., 2021; Tzouanacou et al., 2009). Current literature suggests that
48 NMPs in amniotes (chick, mouse) and anamniotes (fish, frog) are distinct. In amniotes, individual bi-
49 potent NMPs are dual neural/mesodermal fated. In contrast, in anamniotes neuromesodermal
50 competency is maintained in axial progenitors in the tailbud, but individual cells adopt either neural
51 or mesodermal fates. (Attardi et al., 2018; Davis & Kirschner, 2000; Guillot et al., 2021; Martin &
52 Kimelman, 2012; Tzouanacou et al., 2009; Wymeersch et al., 2016).

53 FGF and WNT treatment of pluripotent stem cells *in vitro* generates a population of cells that resemble
54 *in vivo* NMCs both phenotypically and functionally: a high percentage of cells co-express SOX2/TBXT
55 transcription factors, and these populations can differentiate into neural and mesodermal lineages
56 (for a comprehensive list of protocols see Wymeersch et al., 2021).

57 Recent single cell RNA-seq studies have found that *in vitro* cultures harbouring NMC populations are
58 transcriptionally heterogeneous. One interpretation of this data is that *in vitro* NMC populations
59 contain contaminating -non-NMP cells (Edri, Hayward, Baillie-Johnson, et al., 2019; Edri, Hayward,
60 Jawaid, et al., 2019). Alternatively, *Sox2* and *Tbxt* expressing cells themselves are transcriptionally
61 heterogeneous, perhaps reflecting functional heterogeneity. A proportion of in vitro-derived NMP-
62 like cells expressing *Tbxt* (monitored with a fluorescent reporter) have dual potential for neural and
63 mesodermal differentiation (Tsakiridis & Wilson, 2015). However, the bi-potency of individual NMP-
64 like cells co-expressing *Sox2* and *Tbxt* remains unproven.

65 Addressing these questions requires the use of cells that report on both SOX2 and TBXT expression.
66 Previous reporters have employed either knock-in constructs that disrupt the function of these genes
67 (Avilion et al., 2003; Fehling et al., 2003), or are additive transgenics where there is a risk that
68 expression does not accurately mirror endogenous expression (Koch et al., 2017).

69 Here we use a newly generated minimally disruptive mouse embryonic stem cell (mESC) dual
70 *Sox2/Tbxt* gene expression reporter cell line to examine live cell behaviours, population heterogeneity
71 and functional potency of *in vitro* NMP-like cells. Additionally, we show that rapid deceleration of axis
72 elongation in gastruloids on WNT or NOTCH inhibition corresponds in time with *Tbxt* inhibition, while
73 *Sox2* level dynamics are slower. By clonal plating (using Fluorescence-Activated Cell Sorting -FACS) in
74 vitro-derived Sox2/Tbxt- expressing putative NMC populations, we demonstrate that individual
75 *Sox2/Tbxt* dual positive cells are bona fide bipotent progenitors. We uncover previously elusive lateral
76 plate mesoderm potency within descendants of NMPs, an attribute previously shown only at the
77 population level (Row et al., 2018). Interestingly, the *Sox2/Tbxt* co-expressing population is not
78 functionally homogeneous: the levels of *Tbxt*-GFP predict clonal lineage bias towards mesoderm in
79 individual progenitors. This bias is not fixed and can be tuned by the culture conditions and cell
80 substrates, mirroring the *in vivo* plasticity of NMC populations (Wymeersch et al., 2016). Together, we
81 demonstrate previously unsuspected influences on the fate choices of individual NMPs, and provide
82 a robust basis for further investigating these factors.

83

84 **Results**

85 **1. Generation and Validation of STR-KI mESC line: a novel *Sox2/Tbxt* gene expression**
86 **reporter**

87 To characterise the dynamics of neuromesodermal competent population emergence from mESC, we
88 generated a novel dual reporter: Sox2::mCherry; Tbxt::GFP, hereafter named Sox-Tbxt Reporter
89 Knock-In **(STR-KI)**. We employed CRISPR knock-in transgenesis to replace the stop codon of the
90 endogenous gene loci with T2A self-cleavable peptide fluorescent protein fusions, retaining the *Tbxt*
91 and *Sox2* open reading frames in their entirety. This minimises the chance of adverse phenotypic
92 effects of the transgenes and maximises the faithfulness of the reporters (Fig. 1A) (Dewari et al., 2018).
93 High contribution of STR-KI mESCs in embryo chimeras, whose phenotype was normal, demonstrates
94 that the gene targeting was indeed minimally disruptive to SOX2 and TBXT protein function.
95 Furthermore, the fluorescent reporters in pre-streak and somite stage embryos recapitulated the
96 endogenous in vivo expression pattern of *Tbxt* and *Sox2* in mesodermal and neural lineages,
97 respectively (Fig. 1B, Suppl. Fig. 1A,B) (Wymeersch et al., 2016). In pre-streak high contributing
98 chimeras, *Sox2*-mCHERRY was expressed in the entire epiblast whereas *Tbxt*-GFP expression was
99 undetectable (Suppl Fig. 1A). By early somite stages onwards, *Sox2*-mCherry was predominantly
100 restricted to neural tissues, and primordial germ cells at the base of the allantois, whereas *Tbxt*-GFP
101 was expressed in the node, notochord and nascent mesoderm at the posterior end (Fig.1 C and Suppl.
102 1B). Culturing the STR-KI line following established(Gouti et al., 2014)(Gouti et al., 2014) produced

103 mCherry and GFP double positive cells (putative NMP-like cells). Immunostaining of these in vitro-
104 differentiated NMP-like cultures showed that the reporters faithfully co-localised with endogenous
105 SOX2 and TBXT protein in colonies (Fig. 1C, D).

106 We next tracked the reporters' dynamics over a time course of NMP differentiation (Fig. 1 E). Briefly,
107 this entails differentiation of ESC to an epiblast-like state followed by treatment with the WNT agonist
108 CHIR from day (d) 2 onwards (Gouti et al., 2014). Cells apparently moved along a differentiation
109 trajectory from pluripotent ESC (Sox2^{mCherry} high) to a Sox2^{mCherry} low (putative epiblast) state, followed
110 by appearance of Sox2^{mCherry}/Tbxt^{GFP} double positive cells within 3 days, resembling the SOX2 and TBXT
111 level dynamics seen in epiblast NMC-containing regions *in vivo,* where there is heterogeneity at the
112 transcriptional and protein levels for Sox2 and Tbxt, likely denoting their functional potential (French
113 et al., 2024; Wymeersch et al., 2016). At d3, cells exhibited a spectrum of Tbxt^{GFP} levels before exiting
114 the double-positive state towards Sox2^{mCherry} negative Tbxt^{GFP} high mesoderm from d4. Following the
115 established Gouti et al. 2014 protocol with the STR-KI mESC line reproducibly resulted in the
116 production of ~75% of the population co-expressing mCherry and GFP putative NMCs by day 3,
117 consistent with previous reports (Fig. 1F).

Figure 1

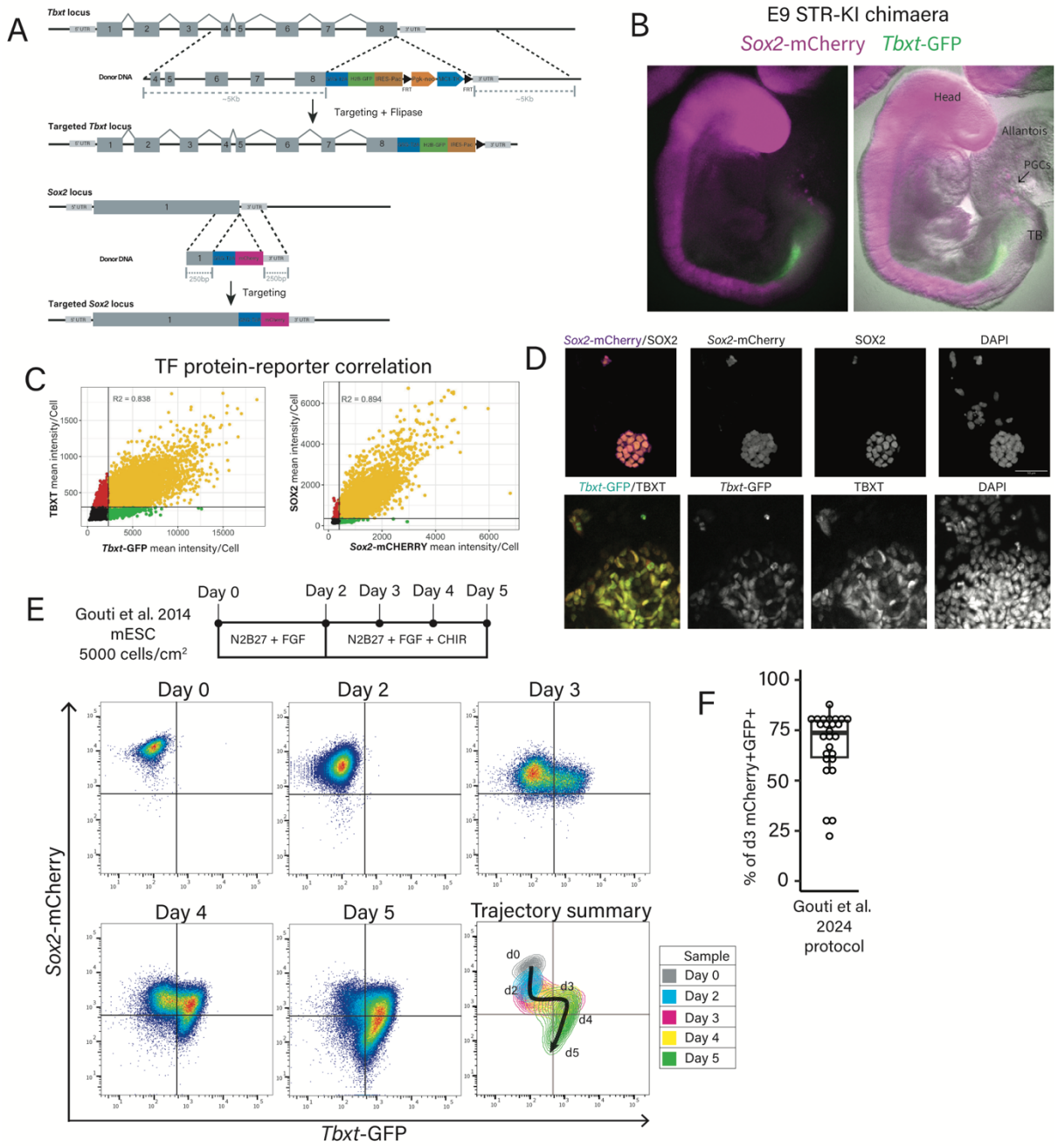

Figure 1. STR-KI, a novel Sox2 and Tbxt mESC fluorescent reporter cell line that allows the study of NMP-like cell differentiation trajectories. A) *Schematic illustration of the targeting construct for the insertion of GFP and mCherry in the Tbxt and Sox2 loci, respectively.* ***B)*** *Embryonic day 9 STR-KI chimaera showing high contribution of STR-KI to the entire embryo and showing appropriate location of the fluorescent reporters. Note high mCherry in neural tissues like brain, neural tube and primordial germ cells (PGCs), whereas GFP labels the notochord and Tailbud (TB).* ***C)*** *Protein correlation between endogenous SOX2 and TBXT transcription factors, and Sox2-mCherry and Tbxt-GFP fluorescent proteins, respectively. Cells for analyses taken from in vitro differentiation assays.* ***D)*** *Example of*

colonies derived from following Gouti et al. 2014 NMP differentiation protocol. Stained for TBXT and GFP, and SOX2 and mCherry to show co-localisation in immunostaining. ***E)*** *Flow cytometry time-course to monitor reporter expression along the Gouti et al. 2014 differentiation protocol from mESC (Day0) into Day 5. A representative example (from n=4) is shown together with a trajectory summary that highlights the population dynamics.* ***F)*** *Efficiency of STR-KI mESC differentiation into NMP-like (Sox2-mCherry and Tbxt-GFP double positive) at Day 3 following Gouti et al. 2014 protocol. n=26*

2. Gene expression and lineage potential analysis of Sox2^{mCherry}/Tbxt^{GFP} fluorescent subpopulations during differentiation

To characterise the cell populations that emerge in the differentiation trajectory, we performed FACS during the differentiation protocol and analysed the gene expression profiles of various populations across the trajectory we identified in Fig. 1E via qPCR of diagnostic marker genes at d2-d4 (Fig. 2A,B; Suppl. 2 A,B). The marker genes analysed were: pluripotency-associated *Nanog*, *Nodal* and *Oct4*; axial progenitor markers *Sox2*, *Tbxt*, *Fgf8*, *Evx1*, *Cdx2*, *Wnt3a* and *Nkx1.2*; paraxial mesoderm marker *Tbx6* and lateral mesoderm marker *Flk-1*; and neural-associated *Otx2, Sox1* and *Pax6*. In all sorted populations, the endogenous gene expression activity of *Sox2* and *Tbxt* was accurately recapitulated by mCherry and GFP transcripts. mCherry transcription was higher in populations that also exhibited high Sox2, remained Tbxt negative and expressed pluripotency or neural markers across all days tested (Sox2^{mCherry}+;Tbxt^{GFP} negative). The putative NMC population (Sox2^{mCherry}+;Tbxt^{GFP}+) displayed relatively constant Sox2-mCherry fluorescence but a spectrum of Tbxt-GFP levels by flow cytometry. To further characterise the expression profile of cells that gradually increase *Tbxt*-GFP fluorescence along the differentiation trajectory, we subdivided the NMC-like population into low (Sox2^{mcherry} + Tbxt^{GFP}-low) and high (Sox2^{mcherry} + Tbxt^{GFP}-high) expressing subpopulations. Since the levels of *Tbxt*-GFP in the double-positive population increased before the appearance of *Tbxt*-GFP single positive mesoderm cells, we hypothesised that low and high NMC-like population represented maturation states within the same population. Specifically, we proposed that high *Tbxt*-GFP positive cells were further along a mesoderm differentiation trajectory than Tbxt-GFP low cells, as suggested *in vivo* (Romanos et al., 2021; Wymeersch et al., 2016). Bulk gene expression analyses by qPCR supported this hypothesis, since although both Sox2^{mcherry}+Tbxt^{GFP} low and high populations expressed similar levels of NMC markers, Tbxt^{GFP} cells were enriched for mesodermal markers such as *Wnt3a* and *Tbx6*, while expression of neural genes like *Sox1* were low. Finally, the absence of Sox2, coupled with the high expression of gene markers like *Tbx6* and *Flk-1* in Sox2^{mCherry} negative Tbxt^{GFP}+ and Sox2^{mCherry} negative Tbxt^{GFP} negative (double negative) populations, together with the gradual

160 downregulation of NMC/caudal markers like *Fgf8* and *Wnt3a* from day 3 to day 4, suggested that these
161 two populations represented nascent and differentiated mesoderm respectively. The expression of
162 pluripotency- and early mesoderm/node marker *Nodal*, together with endoderm markers *Sox17* and
163 *Foxa2* was low, suggesting low-to-negligible fractions of contaminant non-NMC cells. Thus, gene
164 expression in populations undergoing differentiation confirms that our double reporter cell line
165 faithfully recapitulates endogenous gene expression and can be used to purify expected neural,
166 mesodermal and NMC-like cell populations based on *Sox2-mCherry* and *Tbxt-GFP* expression levels
167 (Fig. 2B, Suppl. 2A,B).
168
169 To test whether the apparently dynamic changes in Sox2^{mcherry} and Tbxt^{GFP} cell populations during NMP
170 differentiation (Fig.1 E) represent one or more lineage trajectories, the lineage potentials of sorted
171 subpopulations at day 3 of NMP differentiation were assayed over 3 further days in continuous neural
172 and mesodermal (FGF and CHIR) inducing conditions (Gouti et al., 2014; Tsakiridis & Wilson, 2015)
173 (Fig 2C, Suppl. Fig. 2C). These subpopulations were: 1) Sox2^{mcherry}+ Tbxt^{GFP} negative; 2) Sox2^{mCherry}+
174 Tbxt^{GFP}-low; 3) Sox2^{mCherry}+ Tbxt^{GFP}-high; and 4) Sox2^{mcherry} negative Tbxt^{GFP}+. Sorted populations
175 showed differential responses to these stimuli. Sox2^{mcherry} single positive cells mainly remained single
176 positive. Together with the enrichment of Sox1 in the starting population, this suggests a neural
177 identity for these cells. However, a proportion of the progeny lost expression of both reporters (double
178 negative cells), suggesting that CHIR/FGF induced further differentiation to a Sox2-negative state.
179 Sox2^{mCherry} + Tbxt^{GFP}-low cells also produced Sox2^{mcherry} single positive cells by day 3, but also a
180 recapitulation of the pattern shown in Fig. 1E: emergence of Sox2^{mCherry} + Tbxt^{GFP} -high cells, followed
181 by a high proportion of Sox2^{mCherry} negative Tbxt^{GFP}+ and later double negative cells. This suggests that
182 Sox2^{mCherry} + Tbxt^{GFP}-low NMCs produce both neural and mesodermal cells. Interestingly, Sox2^{mCherry} +
183 Tbxt^{GFP}-high cells produced few Sox2^{mcherry} single positive cells but followed a predominantly
184 mesoderm trajectory, producing a Sox2^{mCherry} negative Tbxt^{GFP}+ and then double negative cells. Finally,
185 Sox2^{mcherry} negative Tbxt^{GFP}+ only produced double negative cells. Together with its enrichment in
186 expression of mesoderm markers, it suggests this is an already mesoderm-committed population.
187 Taken together, using our dual reporter, we have captured the *in vitro* NMC-lineage trajectory of the
188 progenitors and their progeny (Fig 2D, see summary). Interestingly, populations expressing low and
189 high levels of Tbxt^{GFP} at d3 show distinct potency: Sox2^{mCherry} Tbxt^{GFP}-low cells produced a higher
190 proportion of Sox2^{mch} positive neural descendants compared to Sox2^{mCherry} Tbxt^{GFP}-high cells. This
191 supports our hypothesis that the *Tbxt*-high NMC population is predisposed towards mesoderm
192 differentiation. Thus, within the Sox2^{mch}Tbxt^{gfp} double positive NMC population, there are cells with
193 differing competence to differentiate to neural or mesodermal outcomes. It had been suggested that

194 different in vitro NMC-like populations are biased in lineage potential depending on their starting
195 pluripotent state (Edri, Hayward, Baillie-Johnson, et al., 2019). Our data suggests an alternative
196 possibility: that the bias within the NMC-like population depends on the transcriptional state of cells
197 within the same population. Thus, heterogeneous competence to respond to stimuli can affect the
198 outcome of assays testing the functional properties of NMP populations.

199 Treatment of pluripotent cells with FGF and CHIR leads to the expression of both paraxial and lateral
200 mesoderm markers (Edri, Hayward, Baillie-Johnson, et al., 2019; Gouti et al., 2017). Since NMPs
201 predominantly produce paraxial mesoderm, the expression of lateral mesoderm markers has been
202 attributed to other in-vitro derived progenitor populations that emerge alongside NMP-like cells in
203 these protocols. In vivo, while homotopic grafts of NMCs overwhelmingly give rise to paraxial
204 mesoderm (Cambray & Wilson, 2007; Wymeersch et al., 2016), heterotopic grafts to the posterior
205 primitive streak lead to lateral mesoderm differentiation (Row et al., 2018). Theoretically, this result
206 can arise from population heterogeneity or from lateral mesoderm potency of NMPs. To distinguish
207 these possibilities, we subjected FACS-enriched Sox2^{mCherry}+ Tbxt^{GFP}-high cells, containing putative
208 NMP-like cells to examine their potential to produce lateral plate mesoderm lineages. We followed a
209 previously reported protocol, which includes bulk *in vitro* NMP differentiation followed by BMP
210 treatment (Row et al., 2018). Seeding 25 to 1000 Sox2^{mCherry}+ Tbxt^{GFP}-high cells, we observed not only
211 Flk-1 protein labelling in colonies but also the formation of primitive tubes similar to those seen in
212 classical endothelial assays (Taoudi et al., 2005) (Suppl. Fig. 2E). These findings indicate that Sox2/Tbxt-
213 positive NMP-like cells can produce lateral mesoderm, favouring the hypothesis that in vitro NMP-like
214 cells themselves (and not accompanying differentiated cells from other origin) are the source of lateral
215 mesoderm. Thus, we demonstrate a previously unrecognised differentiation potential within enriched
216 Sox2+Tbxt+ populations *in vitro,* mirroring the lineage potential of unsorted Sox2+Tbxt+ regions *in*
217 *vivo* (Row et al., 2018; Wymeersch et al., 2016) .

218 Since our data suggests that we can live-track the lineage potential of *in vitro* derived NMC
219 populations, we hypothesised that we can now test factors that might have an effect in the NMC
220 population differentiation outcomes. Using our STR-KI line we dynamically tracked Sox2 and Tbxt
221 during in mESC-derived gastruloid models of axis elongation. In the standard gastruloid protocols
222 (Baillie-Johnson et al., 2015; van den Brink et al., 2014), aggregates of mESCs grown in N2B27
223 remain Sox2-positive and Tbxt negative until 48 hours post aggregation (hpa), then exit
224 pluripotency. At 48 hours, a 24-hour pulse of CHIR is used to activate WNT globally and ensure
225 robust symmetry breaking. WNT activation nduces Tbxt, transiently in all cells, which then
226 resolves into polarized expression at the posterior pole by 72 hpa and is followed by
227 elongation. We first investigated the dynamics of mesoderm differentiation in gastruloids in the

presence/absence of global WNT activation via CHIR (Suppl. Fig. 2F). After treatment with CHIR, most cells became Tbxt^{GFP} + by 72hpa, and down-regulated Sox2^{mCherry}. In the absence of CHIR, STR-KI cells remained Sox2^{mCherry} high, but a small portion of cells began to express Tbxt^{GFP}. These trends were maintained at the population level by 96hpa (Suppl. Fig. 2F). We also observed general events such as downregulation of Sox2^{mCherry}, symmetry breaking and polarisation of Tbxt^{GFP} to the posterior growing axis only upon the CHIR pulse. Thus, our cell line is suitable for the generation of gastruloids.

We next used STR-KI gastruloids to track the dynamics of reporter expression in gastruloids upon manipulation of signalling pathways with known roles in mesoderm differentiation from NMPs: WNT and Notch(Cooper et al., 2024).We next used STR-KI gastruloids to track the dynamics of reporter expression in gastruloids upon manipulation of signalling pathways with known roles in mesoderm differentiation from NMPs: WNT (Wymeersch et al., 2016) and Notch (Cooper et al., 2024). We treated gastruloids that had broken symmetry and started elongating with either WNT or Notch inhibitors (IWP2 and LY, respectively) and live imaged them every hour for 24 hours to monitor major axis length and changes in reporter expression (Fig. 2E,F). Both inhibition of WNT and NOTCH decelerated major axis growth (elongation) starting as early as between 2 and 3 h post treatment (Fig. 2G).

Segmentation of Sox2^{mCherry} and Tbxt^{GFP} fluorescence in individual cells to determine axial progenitor regions, allowed monitoring of double reporter dynamics during gastruloid axis growth. Treatment with IWP2 or LY rapidly decreased Tbxt^{GFP} signal (within ~2-3h), while Sox2^{mCherry} signal increased after ~10-15 hours, compared to the DMSO control (Fig2. H). This coincides in time with growth deceleration (Fig2. H, I). Thus, the rapid Tbxt^{GFP} signal downregulation coupled with slowdown of axis elongation in response to WNT or NOTCH inhibition suggests AP axis elongation is driven predominantly by *Tbxt*-expressing cells.

Figure 2

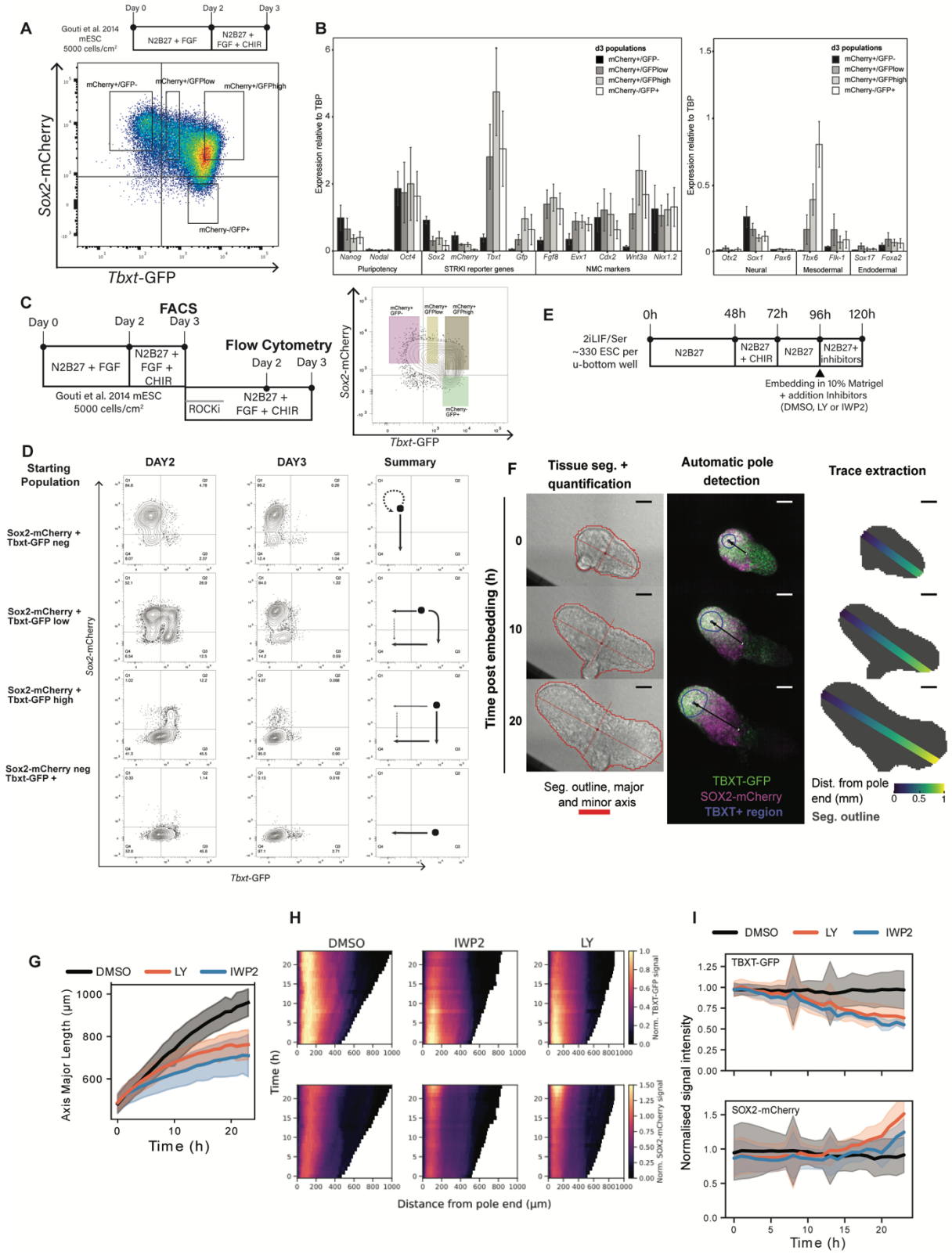

Figure 2. In vitro derived Sox2-mCherry and Tbxt-GFP co-expressing cells are NMCs, and their lineage trajectory can be captured for potency studies. A) *Differentiation protocol scheme and representative gating strategy for FACS and further gene expression analyses performed at day 3 of the differentiation*

protocol. ***B)*** *qPCR gene expression analysis of the populations in A. Gene markers of Pluripotency, Neuromesodermal competent cells (NMC) and differentiated cells (neural, mesodermal, endodermal) were chosen for this characterisation. n=3 per each population* ***C)*** *Differentiation protocol scheme and representative gating strategy for FACS and further time-course lineage potency studies.* ***D)*** *Flow cytometry data on one time-course experiment (see Suppl. Fig 2C for 2 more experiments), following the Sox2-mCherry and Tbxt-GFP expression dynamics. A summary of the lineage outcomes across the time-course and 3 experiments is provided. Thickness of arrows represents contribution to the trajectory of the arrow, dashed arrow indicates a trajectory that is likely to happen given the proportions of cells at the end of the experiment, but we have not formally proven here.* ***E)*** *Experimental set up for the generation of Gastruloids and embedding in 10% matrigel at 96 hours with DMSO, Wnt signaling inhibitor IWP2 (5uM) or Notch signaling inhibitor LY (150nm). Gastruloids were imaged on a confocal microscope every hour for 24 hours after embedding.* ***F)*** *Quantification pipeline of 3D gastruloid confocal image stacks. Whole tissue segmentation of phase contrast confocal images using the Segment anything model (arXiv:2304.02643) and quantification of tissue properties. Then the extending Tbxt-GFP positive pole was automatically detected, shown over a median z-projection of Tbxt-GFP Sox2-mCherry signal. Along this pole orientation, a 50um wide sample trace of the gastruloid was isolated, and the distance from the gastruloid edge was calculated. All scale bars indicate 100um.* ***G)*** *Treatment of gastruloids with IWP2 or LY decreases major axis length of the gastruloid with IWP2 showing a greater effect on gastruloid eccentricity or 'roundness'.* ***H)*** *Heatmaps show the average Tbxt-GFP or Sox2-mCherry signal per binned distance from the end pole along time post Matrigel embedding. Treatment with IWP2 or LY shows a decrease in Tbxt-GFP signal and increase in Sox2-mCherry signal compared to the DMSO control.* ***I)*** *Average intensity of the isolated gastruloid tip reveals a delayed onset of Sox2-mCherry increase in the IWP2 or LY treated conditions in contrast to a near immediate decrease in Tbxt-GFP signal.*

3. Clonal tracing of in vitro derived NMCs reveals balance/bias of NMPs dependent on matrix and T levels

Our findings at the bulk level above suggest there are lineage biases within the NMC (*Sox2/Tbxt* double positive) population and that nuances in *Tbxt* levels influence neural or mesodermal differentiation outcomes. Therefore, we asked whether lineage bias is reflected across the whole *in vitro* NMC-like population or limited to a subset of already lineage-specified cells expressing either the very highest

288 or lowest levels of the reporters. We therefore asked whether the levels of Tbxt (or Sox2 influence the
289 degree of neural versus mesoderm differentiation.
290
291 To track the progeny of individual *Sox2* and *Tbxt* co-expressing cells we used FACS coupled to single-
292 cell deposition into 96-well plates (Fig. 3A). We then correlated this information with the lineage
293 output observed by immunofluorescence and high throughput microscopy in each well after 5 days in
294 culture conditions that support both neural and mesodermal differentiation (Fig. 3B). This
295 experimental set-up allowed for a definitive examination of potency via immunostaining for SOX2 or
296 TBXT at the clonal level in *in vitro* derived NMCs. A variety of substrates are used in different NMC-
297 generating protocols, and we therefore compared the clonal lineage output of Sox2^{mCherry} Tbxt^{GFP} co-
298 expressing cells on fibronectin, gelatin, geltrex and matrigel. Sox2^{mCherry} + Tbxt^{GFP} low and Sox2^{mCherry} +
299 Tbxt^{GFP} high input cells showed distinct lineage output profiles. Sox2^{mCherry} + Tbxt^{GFP} high cells gave rise
300 to a greater proportion of Tbxt^{GFP} only colonies, confirming our previous data showing that the
301 increased mesoderm differentiation in Sox2^{mCherry} + Tbxt^{GFP} high cells at the population level is a
302 function of high TBXT expression in individual cells (Fig3. C). Interestingly, Sox2^{mCherry} + Tbxt^{GFP} high
303 cells also showed higher plating efficiency than Sox2^{mCherry} + Tbxt^{GFP} low cells, suggesting different
304 adhesive properties to the cell substrate (Fig3. C, Suppl. Fig 3A, B). Substrate composition differentially
305 affected cell phenotype: specifically, matrigel led to a large number of colonies where
306 Sox2^{mCherry}Tbxt^{GFP} double positive cells persisted over the culture period. Intriguingly, although the
307 plating efficiency of Sox2^{mCherry} + Tbxt^{GFP} low or high was particularly poor on gelatin, this substrate
308 appeared to enrich for colonies containing double positive cells (Fig3. C, Suppl. Fig. 3A, C).
309 Furthermore, the number of cells per colony was high using gelatin as substrate (Suppl. Fig. 3A), and
310 cells grew as compact colonies rather than dispersed cells, as on other substrates, suggesting that
311 once established from Sox2^{mCherry} + Tbxt^{GFP} low cells, double positive cells are favoured by self-
312 adherent growth. Sox2^{mCherry} + Tbxt^{GFP} high colony survival on geltrex and matrigel was comparable,
313 although matrigel led to more than two-fold higher clone survival of Sox2^{mCherry} + Tbxt^{GFP}-low cells.
314 Cells in the low-to-medium range of Tbxt^{GFP} expression values were abundant enough to permit index
315 sorting, recording the fluorescence intensity of each reporter for individual sorted cells. Thus, we could
316 correlate fates to specific input fluorescence values (Fig 3D). Overall, the trends in differentiation
317 outcome were evident at individual colony level. For example, TbxtGFP high cells either gave rise to
318 TBXT+ or double negative cells, consistent with the population analysis that showed cells express
319 Tbxt^{GFP} transiently before differentiating towards presumptive mesoderm. At lower input values,
320 SOX2+ cells and double positive cells were evident. This confirmed that Sox2^{mCherry} + Tbxt^{GFP} + cells, at
321 least at lower values of TBXT ^{GFP}, are dual potent, and that these ox2^{mCherry} + Tbxt^{GFP} low cells can self

322 propagate but further suggested that the outcomes of differentiation appear to be sensitive to
323 differing levels of TBXT ^{GFP}.
324
325 We next used the low-to-medium level Tbxt^{GFP} index sorted cells to mathematically determine
326 whether the clonal lineage of individual NMP progeny is controlled by the initial levels of Tbxt or *Sox2*
327 expression and the cell substrate. Tbxt^{GFP} and Sox2^{mCherry} expression levels recorded at the time of
328 plating (time = 0), will be designated *T* and *S*, respectively. After 5 days, each of these seeded cells
329 gave rise to varying numbers of cells (n) with four phenotypes based on their expression of TBXT and
330 SOX2: n_{T+S-}, n_{S+T-}, n_{T+S+} and n_{T-S-} .
331 To determine whether the clonal lineage at day 5 post index sort (time = 5 days) was predominantly
332 mesodermal or neural, we compared the difference between numbers of Tbxt^{GFP} and Sox2^{mCherry} (nT+S-
333 versus nT-S+) single positive cells per colony (n_{T+S-} - n_{S+T-}). The histogram of n_{T+S-} - n_{S+T-} determined at
334 time = 5 days, resembled a normal distribution almost centred at n_{T+S-} - n_{S+T-}=zero (Suppl. Fig. 3 E).

335 Of note, many NMPs had small n_{T+S-} - n_{S+T-} values (close to zero) and it would be rather arbitrary to
336 identify these NMPs as mesodermal or neural biased. Instead, the tails of the distribution should
337 correspond with high confidence to mesodermal (n_{T+S-} >> n_{S+T-}) or neural (n_{T+S-} << n_{S+T-}) lineages.
338 Therefore, we used the standard deviation of the distribution as a cut-off to assign NMP lineages, even
339 though this excludes colonies from our analyses. By fitting a Gaussian distribution to the n_{T+S-} - n_{S+T-}
340 data, we estimated a standard deviation of 47 cells (Suppl. Fig. 3 E). Therefore, we classified the lineage
341 of the progeny as mesodermal if n_{T+S-} > n_{S+T} + 47 cells. Conversely, we consider the lineage to be neural
342 when n_{S+T-} > n_{S+T} + 47 cells. To investigate whether the lineage of the NMP progeny at time = 5 days
343 depends on the Tbxt^{GFP} or Sox2^{mCherry} level of the initial index sorted NMP cell at time = 0, we plotted
344 the lineage classification of each seeded NMP as a function of both Sox2^{mCherry} and Tbxt^{GFP}. To
345 implement this, we discretized the scales of Sox2^{mCherry} and Tbxt^{GFP} by selecting bins of equal numbers
346 of colonies.

347 The mesoderm or neural bias of the NMP progeny did not appear to be affected by the level of
348 Sox2^{mCherry} in the Sox2^{mCherry}Tbxt^{GFP} double positive starting population, in line with our experiments
349 at the bulk level and as already suggested *in vivo (French et al., 2024; Kinney et al., 2020; Romanos et*
350 *al., 2021)* (Suppl. Fig. 3 F). In contrast, the starting level of Tbxt^{GFP} strongly influenced
351 neural/mesodermal bias in the clones (Fig. 3D, E). At low values of Tbxt^{GFP}, most NMPs gave rise to
352 neural-biased clones (Fig. 3E). As Tbxt^{GFP} approached a value of 1760 arbitrary units in the index sort,
353 the proportion of NMPs contributing to the mesodermal lineages rapidly increased at the expense of
354 the neural fate (Fig. 3D, E). These results suggest the existence of a Tbxt^{GFP} expression threshold value

355 above which NMP cells are more likely to produce mesodermal cells, in addition to the higher levels
356 of Tbxt^{GFP} (Fig. 3D) at which cells are specified towards mesoderm differentiation.

357 Our results also showed that neural-biased colonies were more abundant on fibronectin and matrigel,
358 whereas we did not observe a particular bias towards either lineage when cells were plated on gelatin
359 or geltrex, suggesting that cell substrate can modulate the outcome of lineage-biased
360 Sox2^{mCherry}Tbxt^{GFP} double positive cells (Suppl. Fig. 3G)

361 To gain mechanistic insight into fate decisions in *in vitro* derived NMPs, we took a modelling approach.
362 We developed a minimal mathematical model of the proliferation and differentiation dynamics of
363 individual NMPs (see Materials and Methods for details). We assumed that each NMP cell can divide
364 symmetrically to: i) self-renew, giving rise to 2 NMPs (SOX2+ TBXT+); ii) differentiate into 2 mesoderm
365 cells (TBXT single positive); iii) differentiate into neuroectoderm, (SOX2 single positive); and iv)
366 differentiate into double negative cells (SOX2 negative TBXT negative). Thus, our model has 4
367 parameters, which are the rates by which NMP cells give rise to each outcome. To check whether the
368 model is sufficient to reproduce the dependence of the neural/mesodermal decision on the initial
369 Tbxt^{GFP} levels in NMPs, we fitted our model to the experimental data.

370 When we grouped NMPs according to cell substrate, we observed that gelatin was associated with
371 the highest rates of self-propagation of NMPs and their differentiation towards mesoderm (SOX2
372 negative TBXT+), as well as descendants of nascent mesoderm, which are double negative (Suppl.Fig.
373 3H). Matrigel, on the other hand, produced the highest rate of differentiation towards neuroectoderm
374 (SOX2+ and TBXT negative) (Suppl.Fig. 3H). When we classified NMPs according to whether they had
375 Tbxt^{GFP} levels below or above the Tbxt^{GFP} threshold reported above (regardless of substrate), we
376 observed that *Tbxt-GFP* values above the threshold lead to a higher differentiation rate towards
377 mesoderm, whereas *Tbxt-GFP* values below the threshold lead to neuroectoderm (Fig. 3.F), consistent
378 with our results shown in Fig. 3E. Interestingly, for both populations, cells produced more NMPs at the
379 highest rates, and cells above the threshold produced NMPs at a higher rate than those below the
380 threshold. This suggests that the threshold in differentiation bias does not affect the ability of NMPs
381 to self-propagate, and distinguishes this lower threshold from the high-Tbxt^{GFP} threshold where cells
382 predominantly exit the NMP state towards mesoderm differentiation. Despite the ability of
383 fibronectin and matrigel to bias cells towards neural differentiation, the mid-level threshold still holds
384 when the experimental data are disaggregated according to the coating used (Supp. Fig. 3I).
385 In summary, clonal analysis and mathematical modelling demonstrates that individual
386 Sox2^{mCherry}Tbxt^{GFP} double positive cells in vitro are NMPs, and that the levels of *Tbxt*, but not *Sox2*,
387 determine whether they are neural-biased, mesoderm-biased or mesoderm-specified. At low to mid-

levels of *Tbxt*, they can self-propagate, but at high levels, they preferentially form mesoderm. The cell substrate can modulate the proportions of neural versus mesoderm cells formed, while gelatin, a relatively challenging substrate for NMP adherence, favours self-adherence and more efficient NMP self-propagation.

392

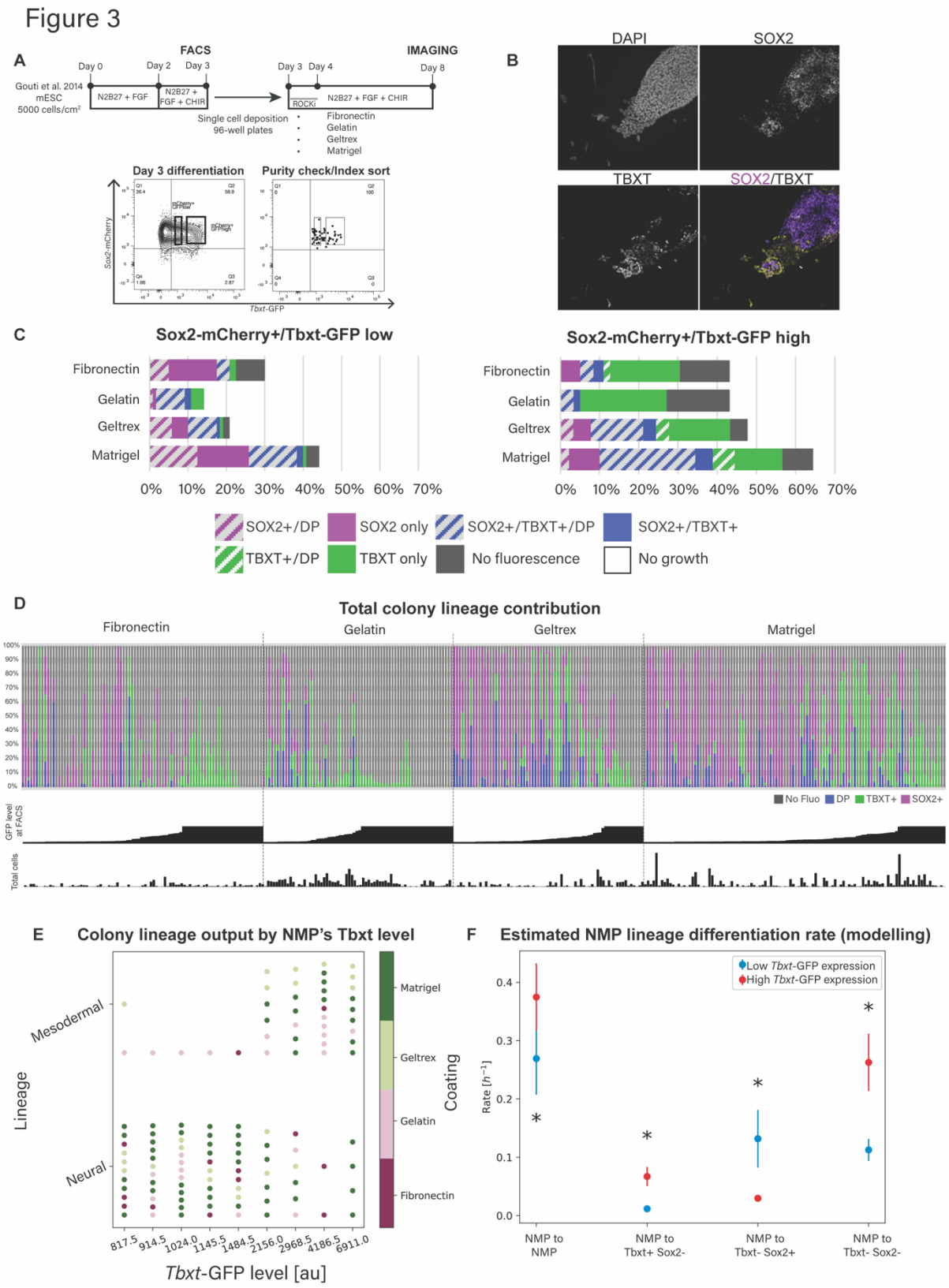

393

394 ***Figure 3. In vitro derived Sox2/Tbxt co-expressing cells are bipotent at clonal level and their lineage***
395 ***output is determined by Tbxt expression. A)*** *Differentiation protocol scheme and representative*
396 *gating strategy for FACS and index sorting according to Sox2^{mCherry} and Tbxt^{GFP} expression. Cells were*

397 *individually seeded into different substrates and cultured further for 5 days. Colony lineage output was*
398 *assessed by immunofluorescence of endogenous SOX2 and TBXT proteins. After imaging, the data was*
399 *analysed by segmenting individual cells in colonies and scoring by their lineage output. as SOX2+,*
400 *SOX2+TBXT+ (Double positive-DP), TBXT+, and no fluorescent (no signal detected).* ***B)*** *Example of a*
401 *colony at the end of the experiment and SOX2 /TBXT stained for imaging.* ***C)*** *Lineage output of colonies*
402 *derived from single cell deposition of sorted Sox2^{mCherry}+Tbxt^{GFP} high and Sox2^{mCherry}+Tbxt^{GFP}. Scoring*
403 *was done as SOX2+, SOX2+TBXT+ (Double positive-DP), TBXT+, and no fluorescent (no signal detected).*
404 *Wells with no colony growth were also scored as 'no growth'. For Sox2^{mCherry}+Tbxt^{GFP} high colonies, n*
405 *scored = 120. For Sox2^{mCherry}+Tbxt^{GFP} low colonies, gelatin and fibronectin n=90, matrigel and geltrex*
406 *n=118.* ***D)*** *Total individual colonies scored with their lineage output, classified by coating and ordered*
407 *by Tbxt-GFP levels at FACS. Total number of cells per colony is also indicated. Note that the plateau in*
408 *GFP levels corresponds to progenitors that were FACS for Sox2^{mCherry}Tbxt^{GFP}high but not index sorted.*
409 *Given the colony lineage output, this corresponds to a high threshold that demarks mesoderm*
410 *commitment.* ***E)*** *NMP lineage output as a function of initial Tbxt^{GFP} levels. Each dot represents one*
411 *colony/experiment. The coating used is shown in colours dark green for matrigel, light green for*
412 *geltrex, pink for felatin and fuchsia for fibronectin. The Tbxt^{GFP} level reported is the middle value in the*
413 *bin.* ***F)*** *Rates estimated with a mathematical model indicating whether the initial individual NMP was*
414 *above (in red) or below (in blue) a Tbxt level threshold of 1760 arbirtary units (au) as function of their*
415 *colony output at the end of the experiment. The dots and the error bars correspond to the mean and*
416 *the standard error of the mean, respectively. stars indicate significant differences ($p < 0.05$) obtained*
417 *after applying a Mann-Whitney statistical test.*

418

419 **Discussion**

420 We report here a new minimally disruptive cell line, STR-KI, that faithfully reports on *Tbxt* and *Sox2*
421 expression. This cell line mirrors endogenous protein expression and minimises phenotypic effects,
422 lending confidence to the studies of lineage dynamics performed here. Reduction in SOX2 function
423 negatively affects ESC maintenance and differentiation (Corsinotti et al., 2017), while reduction of *Tbxt*
424 levels disrupts tail length (Gruneberg, 1958) and cell movement of *Tbxt* +/- cells in chimeras is
425 defective (Wilson et al., 1995). Therefore, it is likely that normal protein function is preserved in this
426 cell line since no abnormal phenotype or distribution of cells was detected in vivo or in vitro.

427 We show here that NMCs generated *in vitro* from mESC (1) are bi-potent and (2) can self-renew in
428 clonal analyses. These are functional attributes used to define *in vivo* NMPs. Our study of the
429 differentiating population over time indicates that ESCs during NMP-like differentiation, while

430 exposed to FGF, first reduce *Sox2-mCherry* expression, as expected in the epiblast *in vivo* (Corsinotti
431 et al., 2017). Then, after CHIR addition, the double positive *Sox2-mCherry Tbxt-GFP* population
432 emerges from these *Sox2-mCherry* low cells. Over the next 48 hours, *Tbxt-GFP* expression increases,
433 until *Sox2-mCherry* expression disappears from *Tbxt*-GFP high cells. *Tbxt-GFP* is later extinguished,
434 resulting in a double-negative population. This cellular trajectory fits well with the known fate of *in*
435 *vivo* epiblast cells that will eventually become NMPs: distal epiblast cells express relatively low *Sox2*
436 levels and exit pluripotency to enter a bipotent NMP state in the caudal lateral epiblast or node-streak
437 border. If they are incorporated in the primitive streak at the midline they will upregulate *Tbxt*,
438 undergo epithelial to mesenchymal transition and exit the streak (and its WNT-high environment) as
439 mesoderm, thereafter downregulating *Tbxt* (French et al., 2024; Kispert et al., 1995; Wymeersch et
440 al., 2016).

441 In vivo, axial elongation is sensitive to perturbation of both WNT and NOTCH signalling, at least partly
442 because NMPs require these pathways for maintenance (WNT) and continued mesoderm production
443 (WNT, NOTCH) (Cooper et al., 2024; Martins-Costa et al., 2024; Wymeersch et al., 2016). TBXT is
444 directly activated by WNT signalling (Yamaguchi et al., 1999) (Yamaguchi et al. 1999), and optimal
445 levels require NOTCH signalling (Cooper et al., 2024), and therefore an effect of inhibiting WNT or
446 NOTCH signalling on TBXT is expected. However, the rapid (2-3h) suppression of $Tbxt^{GFP}$ by both
447 inhibitors, while $Sox2^{mCherry}$ levels were unchanged for 10-15h, indicates gastruloids require both
448 pathways to be intact to maintain high levels of TBXT, and furthermore, the immediate slowing of
449 gastruloid axial elongation suggests that mesoderm production by TBXT is a key driver of continued
450 gastruloid elongation.

451

452 We show that single *Tbxt/Sox2* expressing cells are capable of differentiation towards SOX2-positive
453 neurectoderm and TBXT-positive (and subsequently double-negative) mesoderm. This formally
454 demonstrates that double-positive cells generated using standard protocols from mESC are bipotent
455 NMPs. Interestingly, however, we have also shown, through indexing double positive cells during
456 sorting, and mathematical modelling of the outcomes, that higher $Tbxt^{GFP}$ levels predispose cells
457 towards mesoderm differentiation. This seems to occur at two distinct levels of $Tbxt^{GFP}$. Firstly, double-
458 positive cells with the highest $Tbxt^{GFP}$ fluorescence appear specified for mesoderm differentiation,
459 reminiscent of a minority of cells at the primitive streak which express high levels of TBXT yet still
460 express SOX2, but are not bipotent on transplantation to NM-fated regions (Cambray & Wilson, 2007;
461 French et al., 2024). Secondly, a threshold, mid-level of GFP appears to bias, but not commit, cells to
462 a mesoderm fate. This is unexpected because in vivo NMCs, even from predominantly mesoderm-

463 fated regions (which express higher TBXT than those in neural-fated regions), are still potent to
464 produce neurectoderm on transplantation to more neural-fated regions (French et al., 2024;
465 Wymeersch et al., 2016). Our study suggests that a previously hidden nuance exists within the *in vitro*
466 derived NMC population, whereby SOX2/TBXT-positive NMCs exhibit (at least) three functional
467 phenotypes: neural-biased, mesoderm-biased and mesoderm-specified. The primacy of TBXT dosage
468 in influencing the outcome of differentiation recalls previous experiments in vivo where levels of TBXT
469 dictated cell behaviours: cells stay in the primitive streak/tail bud at low TBXT dosage, and exit as
470 mesoderm at higher doses (Wilson & Beddington, 1997; Wilson et al., 1995). Our study indicates that
471 this works at individual cell level, whereby cells sense cues in their environment (e.g. WNT, NOTCH),
472 respond by tuning TBXT up or down, which in turn influences the differentiation outcome at single cell
473 level.

474

475 In conclusion, this dual reporter ESC line provides new opportunities to develop strategies for the
476 study of the molecular mechanisms underlying self-renewal and differentiation of NMPs.

477

478 **Materials and methods**

479 Reporter mESC Generation

480 To generate the double reporter, we performed CRISPR transgenesis in two targeting rounds (one for
481 each gene locus) in E14tg2a ESC following a stablished protocol (Dewari et al., 2018). The donor DNA
482 and sgRNA are listed in Table S1. Briefly, we replaced the stop codon at the C-terminus of the targeted
483 genes by homology recombination with a reporter gene containing T2A-mCherry (in the case of Sox2)
484 or T2A-H2B-GFP (in the case of *Tbxt*). The *Tbxt* targeting vector contained a puromycin resistant
485 cassette which was used for clone selection. *Sox2*+ Selection was performed by FACS of individual
486 mCherry+ cells into 96-well plates. Single clones were picked, expanded, and checked for correct
487 transgene integration by PCR and Sanger sequencing.

488

489 Chimaera generation

490 C57BL/6 female mice (Charles River) were superovulated (100 IU/ml PMSG and 100 IU/ml hCG
491 intraperitoneal injections 48 h apart) and crossed with wild-type stud male mice. Pregnant mice were
492 culled at embryonic day 2.5 (E2.5) by cervical dislocation, ovaries with oviducts were dissected and
493 collected in pre-warmed M2 medium. Oviducts were flushed using PBS and a 20-gauge needle
494 attached to a 1 ml syringe and filled with PB1 (Whittingham, 1974). E2.5 embryos were collected and

495 washed in PB1, their zona pellucida removed using acidic Tyrode's solution and transferred to a plate
496 with incisions where two clumps of approximately eight sender and eight receiver cells were added to
497 each embryo. Embryos were then incubated at 37°C in 5% CO2 for 48 h prior to fixation, or for 24h
498 prior to transfer to pseudopregnant females for the generation of post-implantation chimaeras.
499 Females carrying the transferred embryos were culled following schedule 1 procedures and chimaeric
500 embryos taken out for analyses. The sex of embryos used in this study was not determined. All
501 reagents are listed in Table S1

502

503 Cell culture, differentiation and flow cytometry

504 Double reporter mESCs were maintained on 0.1% gelatin-coated plates in Glasgow Minimum Essential
505 Medium (GMEM, Sigma-Aldrich #G5154) supplemented with 10% foetal calf serum (Gibco #10270-
506 106), 100 U/mL LIF (made in-house), 100µM 2-mercaptoethanol (Gibco #31350-010), 1X non-essential
507 amino acids (Gibco #11140-035), 2mM L-Glutamine (Invitrogen #25030-024) and 1mM Sodium
508 Pyruvate (Invitrogen #11360-039). mESC were passaged every other day with 1X trypsin (Sigma
509 #59429C) after washing with PBS.

510 For NMP differentiation, following Gouti et al. 2014, reporter mESCs were plated at a density of 5.000
511 cells/cm2 on 0.1% gelatin-coated plates in N2B28 medium (1:1 mixture of Neurobasal (Thermofisher
512 #21103049) and Advanced Dulbecco's Modified Eagle Mediu F12 (Thermofisher #12634028)
513 supplemented with 2 mM L-Glutamine, 50 µM 2-mercaptoethanol, 0.5X B27 (Thermofisher
514 #17504001) and 0.5X N2 (Thermofisher #17502048). Cells were supplemented with 10 ng/mL FGF2
515 (R&D Systems #3718-FB) for 48 hours, and for 24 additional hours with both 10 ng/mL FGF2 and 5µM
516 CHIRON99021 (Axon #1386).

517 For single cell plating experiments, differentiated cells were detached using TrypLE Express Enzyme
518 1X (Gibco 12604013) and sorted on CellCarrier 96-well plates coated with 0.1% gelatin, 16.6 µL/mL
519 fibronectin (Sigma #F1141) in PBS, 200 µg/mL Matrigel (Corning #354277) in PBS or 120 µg/mL geltrex
520 (Thermofisher #A1413201) in advanced DMEM/F12, for 1 hour at 37ºC. Cells were cultured in N2B27
521 supplemented with 100 U/mL penicillin/streptomycin (Invitrogen, #15140-122)), 10 µM ROCK
522 inhibitor Y-27632 (Tocris #1254/10) and either 10 ng/mL FGF2 or both 10 ng/mL FGF2 and 5µM
523 CHIRON99021. After 24 hours, media was changed without ROCK inhibitor. The ROCK inhibitor Y-
524 27632 is used to enhance survival of single cells (Watanabe et al., 2007) and we use it in FACS
525 experiments as a means of counteracting dissociation and cell stress induced apoptosis.

526 All cells were maintained under standard culture condition (37ºC and 5% CO2).

527 For flow cytometry and FACS analysis, cells were detached using trypsin on mESC or TrypLE on
528 differentiated cells, quenched and pelleted by centrifugating at 300 g for 3 minutes. For flow
529 cytometry analysis, cells were resuspended in 2% FCS in PBS with 0.1 µg/Ml Draq7 and kept in ice. For
530 FACS sorting single cells, cells were resuspended in N2B27 with 0.1 µg/mL Draq7.

531 Cells were analysed with 4 laser LSR Fortessa (BD) flow cytometer using B 530/30-A, Y/G 610/20-A,
532 and R780/60-A laser/filter combinations or sorted with Cell Sorter BD FACS Aria II using B 525/50-A,
533 Y/G 610/20-A, and R780/60-A laser/filter combinations.

534

535 qPCR

536 200 cells were sorted into PCR tubes containing 10 µL of 2X Reaction Mix (CellsDirect One-Step qRT-
537 PCR Kit; Invitrogen #11753100) with 0.4U/µl of RNAse inhibitor (Invitrogen #AM2694) and flash-frozen
538 on dry ice. Reverse transcription reactions were performed using the Superscript III RT/Platinum Taq
539 mix (CellsDirect One-Step qRT-PCR Kit; Invitrogen #11753100). qPCR was performed using the
540 LightCycler 480 SYBR Green I Master (Roche, #4887352001) in LightCycler 480 Multiwell Plate 384
541 (Roche #04729749001) using the Roche LightCycler 480 Real-time PCR System. TATA-box binding
542 protein (TBP) gene was used as an endogenous control and relative gene expression was calculated
543 using the 2-ΔΔCt method.

544

545 Immunocytochemistry and microscopy

546 Cells were fixed with 4% paraformaldehyde for 10 minutes, washed with PBS two times for a total of
547 10 minutes and permeabilised with 0.5% Triton X-100 in PBS for 10 minutes. After washing two times
548 with PBS, cells were blocked for 30 minutes with 5% donkey serum and 0.1% Triton X-100 in PBS.
549 Primary antibodies in blocking solution were added overnight at 5ºC. After washing two times with
550 PBS, secondary antibodies diluted in blocking solution were added for 2 hours at room temperature.
551 Cells were washed 2 times in PBS and DAPI diluted in PBS was added for 5 minutes at room
552 temperature. Finally, cells were washed two times with PBS. Imaging of the 96-well plates was
553 performed using the High-Content Imaging Opera Phenix Plus from the IRR Imaging Core Facility.
554

555 Gastruloid culture and live imaging

556 Gastruloid culture was carried out as previously described (van den Brink et al., 2020 Vianello et al
557 2020 [dx.doi.org/10.17504/protocols.io.9j5h4q6]). 2i/LIF/FCS CELL LINE cells are washed in PBS before

558 adding 0.05% Trypsin EDTA solution. After ES colony detachment, 5-10 volumes of fresh 2i/LIF/FCS
559 were added to quench the Trypsin EDTA solution. The cells and media were transferred to a universal
560 tube and pelleted by centrifugation at 300g for 3 minutes. The media was aspirated, and the pellet
561 was resuspended in cold PBS to create a single cell suspension. This PBS wash was repeated once
562 more, then the cell pellet was resuspended in prewarmed N2B27 to create a single cell solution. The
563 cells were then counted and then diluted to a solution of 8,250 cells/mL in N2B27 medium. 40µL of
564 this medium, containing ~330 cells, was plated into untreated u-bottom 96 wells and incubated for 48
565 hours at 36 °C and 5% CO2. At 48 hours, 150µL of N2B27 and 3uM CHIR99021 (Axon) were added into
566 the well, the last half of the media was expelled forcefully to dislodge the aggregate but without
567 spilling the medium. The aggregates were cultured for a further 24 hours to Day 3, after which 150µL
568 of media was removed and replaced with 150µL fresh N2B27. At Day 4, gastruloids were washed in
569 N2B27 and then transferred to flat-bottom and black-walled 96-well plates (PerkinElmer) containing
570 ice-cold N2B27 + 10% Matrigel supplemented with LY 411575 (150nM), IWP2 (2.5µM), or an equal
571 amount of DMSO. Gastruloids were left for 5 minutes to drop to the bottom of the well and then
572 placed into an incubation chamber at 36 °C and 5% CO2 to set the Matrigel. After this period,
573 gastruloids were imaged on a confocal microscope (Opera Phenix Plus) every hour for 24 hours.
574 Transmitted light and fluorescence signal was collected using epifluorescence and a 20x objective.
575 Excitations of 488nm and 561nm, emissions of 522nm and 599nm, and exposure times of 0.1s and
576 0.2s were used for GFP and mCherry respectively. Voxel dimensions were 0.89x0.89x5 microns.

577

578 Gastruloid image analysis

579 Image analysis was performed in python using custom scripts and open source libraries. Whole tissue
580 segmentation masks were generated using with the Segment Anything Model (SAM). Extending poles
581 of gastruloids were inferred by median projecting *Tbxt*-GFP signal z-stacks to 2D, smoothing with a
582 Gaussian filter, and isolating pixels over the 90th percentile. Traces were collected in a 50µm wide
583 linear line with an orientation defined by the gastruloid mask centroid to the extending-pole centroid.
584 Extending pole "ends" were isolated as a bin between 80um and 160um from the end of the pole.

585

586 Mathematical modelling

587 In this study, we propose a minimal mathematical model of the dynamics of NMP cells and their
588 progeny to investigate the cell fate decision process. The main assumption is that each NMP cell
589 divides symmetrically, resulting in i) 2 NMPs, or ii) 2 cells that are simultaneously T+ and Sox2-, or iii)

2 cells that are simultaneously T- and Sox2+, or iv) 2 cells that are simultaneously T- and Sox2-. We also assume that, with the exception of NMPs, the other cells do not divide within the time window of our study. The model is encoded in the following linear system of ordinary differential equations describing the time course of NMPs and their progeny:

$$\frac{dNMP}{dt} = \alpha * NMP - \beta * NMP - \gamma * NMP - \delta * NMP \quad \text{(Eq. 1)}$$

$$\frac{dn_{S+T-}}{dt} = 2 * \beta * NMP \quad \text{(Eq. 2)}$$

$$\frac{dn_{S-T+}}{dt} = 2 * \gamma * NMP \quad \text{(Eq. 3)}$$

$$\frac{dn_{S-T-}}{dt} = 2 * \delta * NMP \quad \text{(Eq. 4)}$$

Where *t* is time, *NMP*, n_{S+T-}, n_{S-T+} and n_{S-T-} are the number of NMPs, the number of cells that are simultaneously Sox2+ and T-, the number of cells that are simultaneously Sox2- and T+ and the number of cells that are simultaneously Sox2- and T-, respectively. The model has 4 parameters: α, β, γ and δ, which correspond to the rates at which NMP cells give rise to more NMP cells, cells positive for Sox2 but negative for T (*i.e.*, neural lineage), cells negative for Sox2 but positive for T (*i.e.*, mesodermal lineage) and cells negative for both Sox2 and T (double negative).

To test whether the model was sufficient to reproduce the dependence of the neural/mesodermal decision on the *T* level of the NMP, we fitted the model to the experimental data.

This system has an analytical solution given by

$$NMP(t) = NMP_0 * e^{(\alpha-\beta-\gamma-\delta)t} \quad \text{(Eq. 5)}$$

$$n_{S+T-}(t) = \frac{2*\beta*NMP_0*e^{(\alpha-\beta-\gamma-\delta)t}}{(\alpha-\beta-\gamma-\delta)} + n_{S+T-0} \quad \text{(Eq. 6)}$$

$$n_{S-T+}(t) = \frac{2*\gamma*NMP_0*e^{(\alpha-\beta-\gamma-\delta)t}}{(\alpha-\beta-\gamma-\delta)} + n_{S-T+0} \quad \text{(Eq. 7)}$$

$$n_{S-T-}(t) = \frac{2*\delta*NMP_0*e^{(\alpha-\beta-\gamma-\delta)t}}{(\alpha-\beta-\gamma-\delta)} + n_{S-T-0} \quad \text{(Eq. 8)}$$

Where NMP_0 is the initial number of NMP cells, n_{S+T-0} is the initial number of Sox2 positive but T negative cells, n_{S-T+0} is the initial number of Sox2 negative but T positive cells and n_{S-T-0} is the initial number of double negative cells.

Finally, we assume the following initial condition, reflecting the experiments described in section 3.

$$NMP_0 = 1 \quad \text{(Eq. 9)}$$

616 $n_{S+T-_0} = 0$ (Eq. 10)

617 $n_{S-T+_0} = 0$ (Eq. 11)

618 $n_{S-T-_0} = 0$ (Eq. 12)

619 To fit the model to the experimental data, we minimized the distance function δ between the
620 experimental number of cells and the model predicted number of all cell types for each experiment.
621 The distance d was defined as:

622 $\delta = \sqrt{(NMP_e - NMP_t)^2 + \left(n_{S+T-_e} - n_{S+T-_t}\right)^2 + \left(n_{S-T+_e} - n_{S-T+_t}\right)^2 + \left(n_{S-T-_e} - n_{S-T-_t}\right)^2}$ (Eq.
623 13)

624 Where NMP_e and NMP_t are the experimental and model predicted number of NMP cells, n_{S+T-_e} and
625 n_{S+T-_t} are the experimental and model predicted number of cells positive for SOX2 but negative for
626 TBXT, n_{S-T+_e} and n_{S-T+_t} are the experimental and model predicted number of cells positive for T but
627 negative for SOX2, and finally n_{S-T-_e} and n_{S-T-_t} are the experimental and model predicted number
628 of cells negative for both SOX2 and TBXT. From all best-fitting parameter values that minimized d for
629 each experiment, we calculated the mean and standard error of the mean.

630 A Jupyter Notebook (http://jupyter.org/) containing the source code used to generate the
631 mathematical model plots in Fig. 3 and Supp. Fig. 3 can be found at Zenodo (Ceccarelli & Chara, 2024).

632

633

634

635 Table S1

Reagent	Source	Identifier or catalog number
DNeasy Blood & Tissue Kit	QIAGEN	69504
Q5® Hot Start High-Fidelity 2X Master Mix	BioLabs	M0494S
Agarose	Invitrogen	16500-500
SYBR™ Safe DNA Gel Stain	Invitrogen	S33102
Zymoclean Gel DNA Recovery Kit Protocol	Zymo Research	D4001
Qubit 1X dsDNA HS Assay Kit	Invitrogen	Q33230
Glasgow Minimum Essential Medium	Sigma-Aldrich	G5154
Foetal calf serum	Gibco	10270-106
LIF	Nade in-house	N/A

2-mercaptoethanol	Gibco	31350-010
Non-essential amino acids	Gibco	11140-035
L-Glutamine	Invitrogen	25030-024
Sodium Pyruvate	Invitrogen	11360-039
Trypsin	Sigma	59429C
Neurobasal	Thermofisher	21103049
Advanced Dulbecco's Modified Eagle Mediu F12	Thermofisher	12634028
B27	Thermofisher	17504001
N2	Thermofisher	17502048
FGF2	R&D Systems	3718-FB
CHIRON99021	Axon	1386
TrypLE Express Enzyme 1X	Gibco	12604013
Fibronectin	Sigma	F1141
Matrigel	Corning	354277
Geltrex	Thermofisher	A1413201
Penicillin/streptomycin	Invitrogen	15140-122
ROCK inhibitor Y-27632	Tocris	1254/10
2X Reaction Mix (CellsDirect One-Step qRT-PCR Kit)	Invitrogen	11753100
RNAse inhibitor	Invitrogen	AM2694
Superscript III RT/Platinum Taq mix (CellsDirect One-Step qRT-PCR Kit)	Invitrogen	11753100
LightCycler 480 SYBR Green I Master	Roche	4887352001
LightCycler 480 Multiwell Plate 384	Roche	04729749001

Acknowledgements

The authors thank the IRR core facilities for their important contributions to this work, particularly The IRR Flow cytometry, Tissue Culture and High content Facilities.

Competing interests

No competing interests declared.

Funding

This work was supported by the Medical Research Council (MR/S008799/1 to A.B-C, A.G., V.W, MR/K011200E.K, F.C.K.W), Carnegie Trust for the Universities of Scotland (RIG012666 to A.B-C), the Agencia Nacional de Promoción Científica y Tecnológica of Argentina (PICT-2019-03828 to A.S.C. and O.C), Biotechnology and Biological Sciences Research Council (BB/X014908/1 to O.C.), Wellcome Trust

647 Senior Fellowship (220298 to M.F., J.A. and S.L), Erasmus Exchange fund (to A.G. and D.L.R), Gurdon
648 summer studentship (to A.G).

649 **Data availability**

650 Data availability: All relevant data can be found within the article and its supplementary information.
651

652 **Supplementary Figures**

Suppl. Figure 1

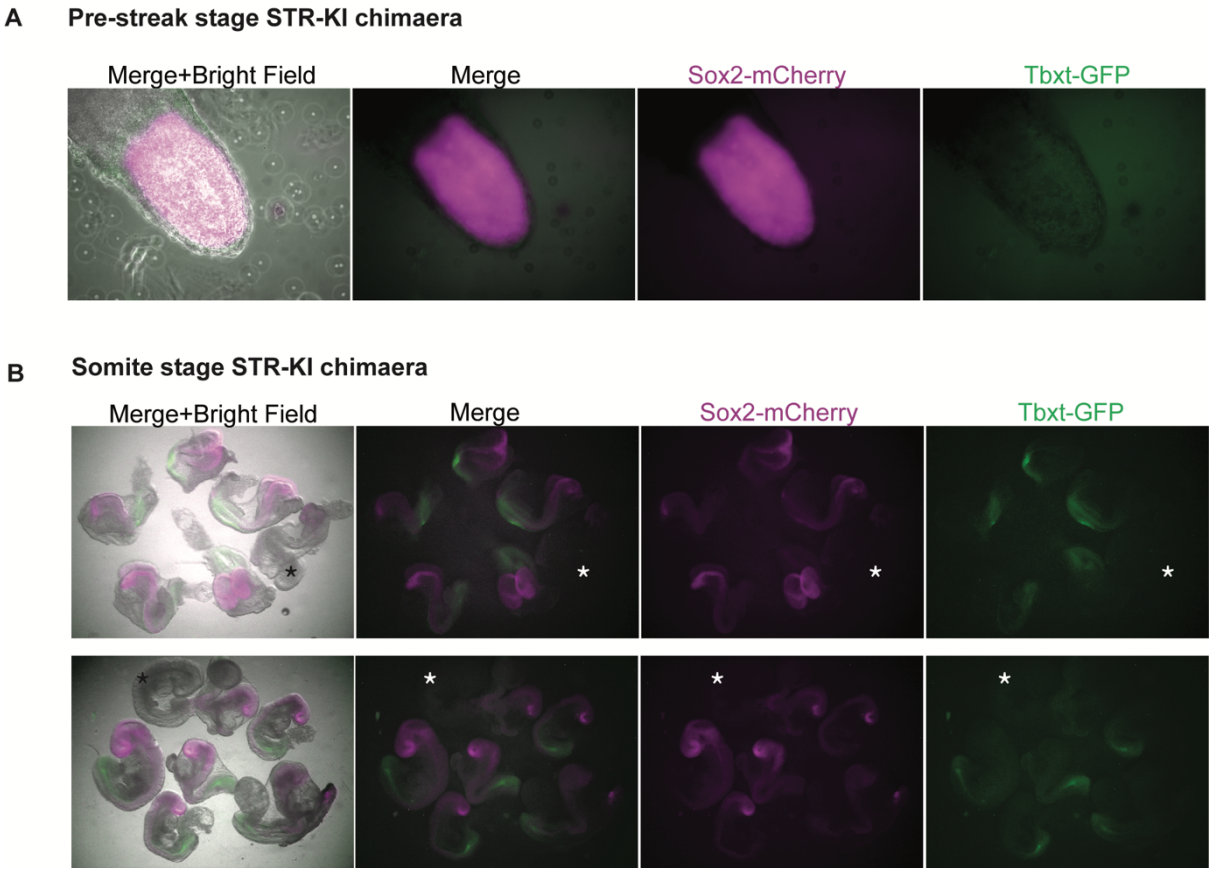

653

654 **Suppl. Figure 1. STR-KI cell line contributes highly to chimaeras. A)** mouse **p**re-streak and **B) E8.5 (2-**
655 **6)** somite stage chimeras appear morphologically normal, show high contribution of STR-KI cells, and
656 correct location of the reporter fluorescent proteins. Asterisk in B shows a non-contributing littermate
657 as negative control.

Suppl. Figure 2

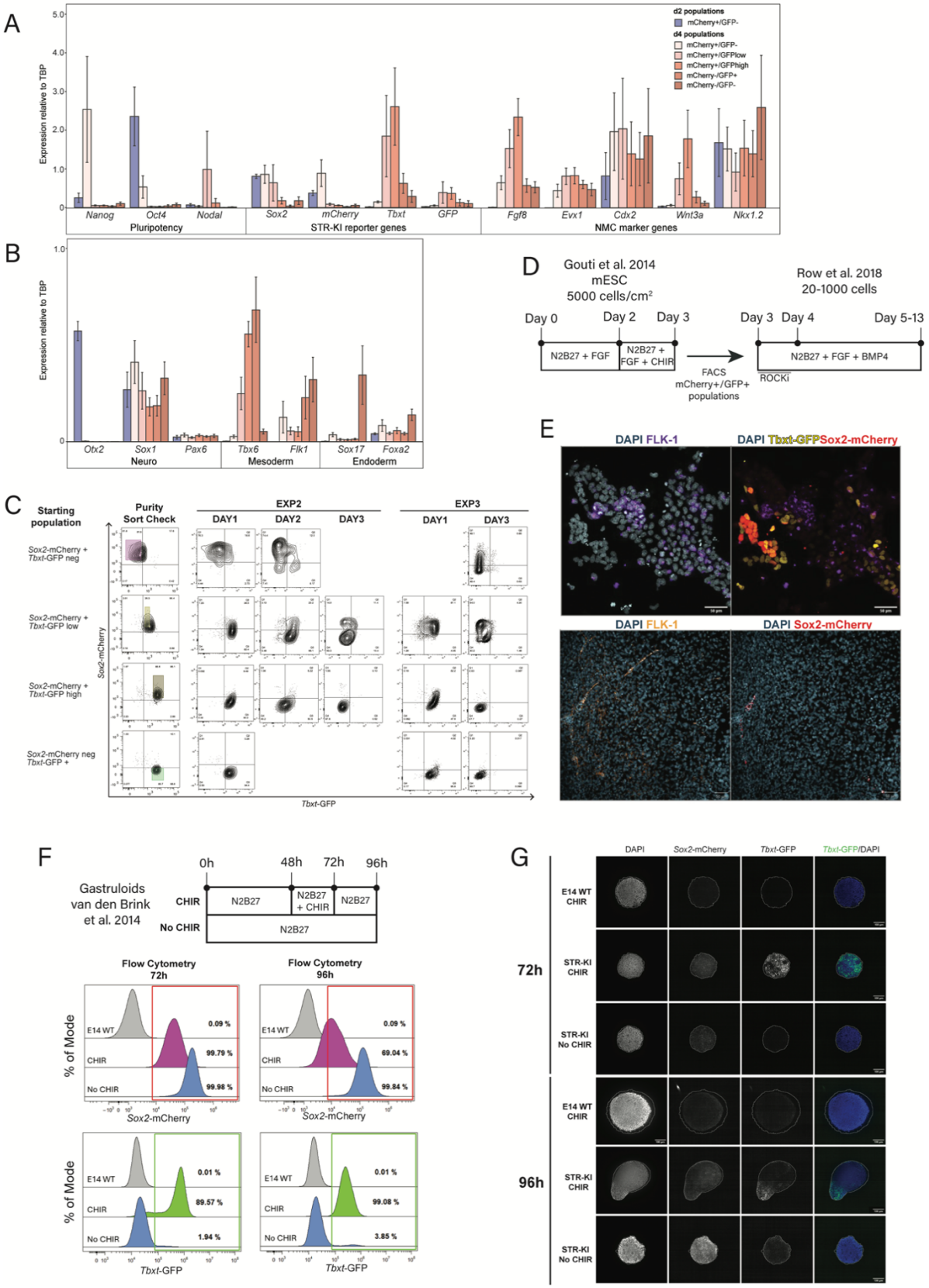

658

659

660 **Suppl. Figure 2. *In vitro* derived *Sox2*-mCherry and *Tbxt*-GFP co-expressing cells are NMC**
661 **progenitors, and their lineage trajectory can be captured for potency studies**
662 **A)** qPCR gene expression analysis of populations on day 2 and day 4 using the same gating strategy
663 and differentiation protocol in Fig2A. Classical gene markers of Pluripotency, Neuromesodermal
664 competent cells (NMC) and differentiated cells (neural, mesodermal, endodermal) were chosen for
665 this characterisation. n=3 per each population **C)** Differentiation protocol scheme and representative
666 gating strategy for FACS and further time-course lineage potency studies. **D)** Repeats of the time-
667 course experiment described in Fig. 2C-D, note the variability between 3 experiments, which is
668 inherent to the differentiation protocol. However, cell populations did follow the same trajectory
669 trends (summarised in Fig. 2D). A representative purity check of the initial FACS populations is shown.
670 **D)** Scheme of the experimental set up for FACS *Sox2*^{mCherry}*Tbxt*^{GFP} double positive progenitors and
671 testing of lateral plate mesoderm (LPM) potency. **E)** Example of colonies stained for the LPM marker
672 Flk-1. In some cases, cells within colonies were Flk-1+ without changes in morphology (top) whereas
673 in other cases elongated Flk-1+ cells were observes, which could indicate endothelial cell
674 differentiation. **F)** Experimental setup for the generation of gastruloids to test symmetry breaking and
675 *Tbxt*^{GFP} activation upon CHIR activation. Flow cytometry on an average of 60 gastruloids were pooled
676 and bulk analysed for 72hpa and 30 gastruloids for 96hpa. n=1 **G)** Immunostaining of Wild type (WT)
677 or STR-KI derived gastruloids for *Sox2*^{mCherry} and *Tbxt*^{GFP} at 72h and 96h. Note the absence of Tbxt^{GFP} in
678 both WT and no CHIR treated gastruloids. Axis elongation is visible between 96-120, depending on the
679 cell line use. STR-KI does show elongation at 96h upon CHIR treatment.

Suppl. Figure 3

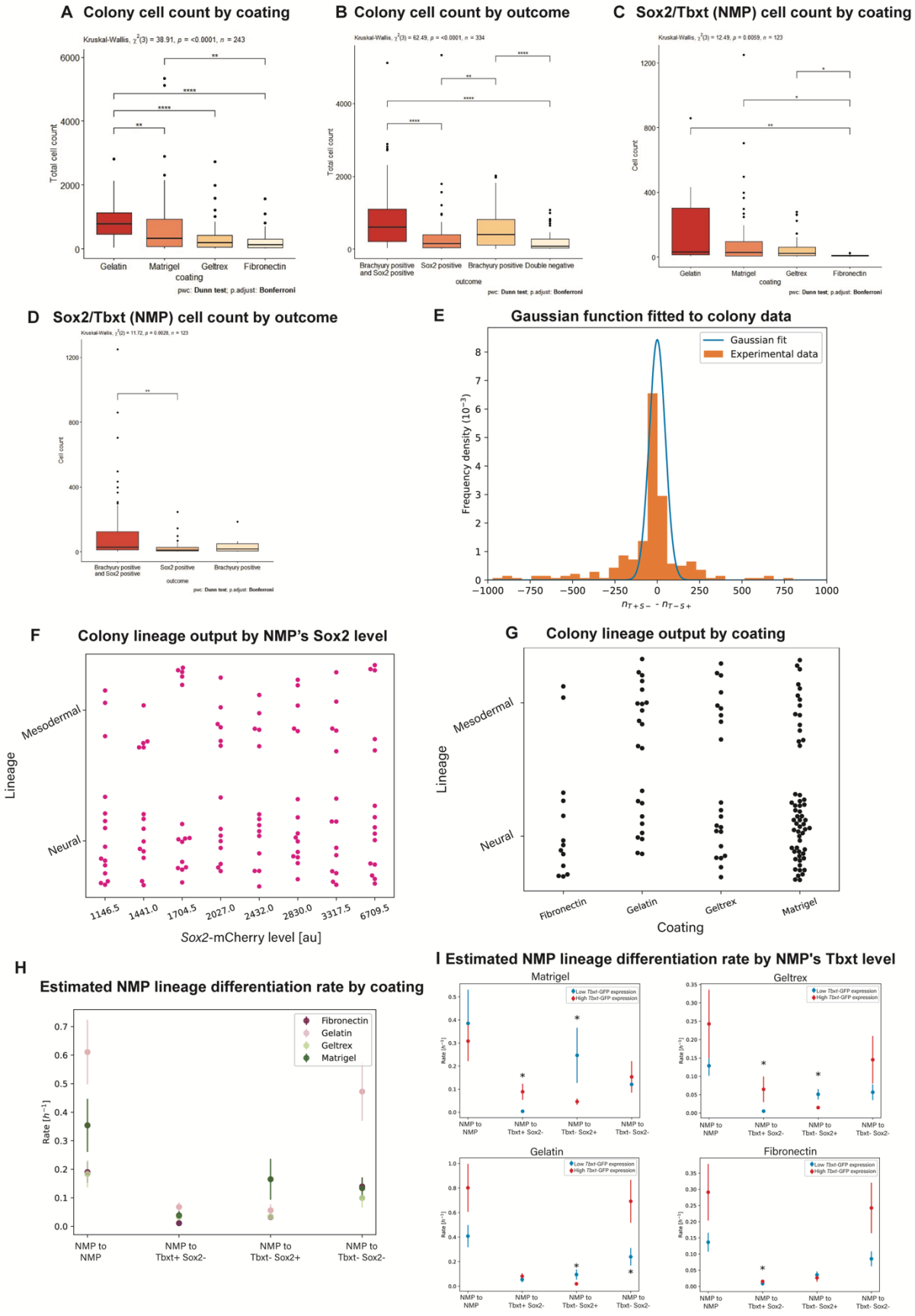

680

681

682 **Suppl. Figure 3. Quantitative analysis and mathematical modelling of clone data.**

683 A) Number of cells per colony segregated by coating. B) Number of cells per colony segregated by
684 colony phenotype. C) number of SOX2+TBXT+ cells per colony by coating. D) number of SOX2+TBXT+
685 cells per colony by colony phenotype. **E)** Histogram for n_{S-T+} - n_{S+T-}. The blue line is the gaussian function
686 fitted to the data. **F)** Clonally plated Sox2 ^{mCherry} Tbxt^{GFP} (NMP) lineage output as a function of Sox2^{mCherry}
687 levels in individually plated NMPs. Each dot represents one colony/experiment. The Sox2^{mCherry} level
688 reported is the middle value in the bin. **G)** Clonally plated Sox2 ^{mCherry} Tbxt^{GFP} (NMP) lineage output as
689 a function of the coting used. **H)** Rates estimated with a mathematical model, coloured by coating
690 used: dark green for matrigel, light green for geltrex, pink for gelatin and fuchsia for fibronectin. Dots
691 are the mean value obtained, and the error bars show the standard error of the mean. **I)** Rates
692 estimated with a mathematical model disaggregated by coating used: fibronectin, gelatin, geltrex and
693 matrigel. The initial NMP cells were above (in red) or below (in blue) a *Tbxt*^{GFP} level threshold of 1760
694 arbitrary units (au). The dots are the mean value obtained, and the error bars show the standard error
695 of the mean. Stars indicate significant differences ($p < 0.05$) obtained after applying a Mann-Whitney
696 statistical test.

697

698 **References**

699 Attardi, A., Fulton, T., Florescu, M., Shah, G., Muresan, L., Lenz, M. O., Lancaster, C., Huisken, J., van
700 Oudenaarden, A., & Steventon, B. (2018). Neuromesodermal progenitors are a conserved
701 source of spinal cord with divergent growth dynamics. *Development*, *145*(21).
702 https://doi.org/10.1242/dev.166728
703 Baillie-Johnson, P., van den Brink, S. C., Balayo, T., Turner, D. A., & Martinez Arias, A. (2015).
704 Generation of Aggregates of Mouse Embryonic Stem Cells that Show Symmetry Breaking,
705 Polarization and Emergent Collective Behaviour In Vitro. *J Vis Exp*(105).
706 https://doi.org/10.3791/53252
707 Binagui-Casas, A., Dias, A., Guillot, C., Metzis, V., & Saunders, D. (2021). Building consensus in
708 neuromesodermal research: Current advances and future biomedical perspectives. *Current*
709 *Opinion in Cell Biology*, *73*, 133-140. https://doi.org/10.1016/j.ceb.2021.08.003
710 Cambray, N., & Wilson, V. (2007). Two distinct sources for a population of maturing axial
711 progenitors. *Development*, *134*(15), 2829-2840. https://doi.org/10.1242/dev.02877
712 Cooper, F., Souilhol, C., Haston, S., Gray, S., Boswell, K., Gogolou, A., Frith, T. J. R., Stavish, D., James,
713 B. M., Bose, D., Kim Dale, J., & Tsakiridis, A. (2024). Notch signalling influences cell fate
714 decisions and HOX gene induction in axial progenitors. *Development*, *151*(3).
715 https://doi.org/10.1242/dev.202098
716 Corsinotti, A., Wong, F. C., Tatar, T., Szczerbinska, I., Halbritter, F., Colby, D., Gogolok, S., Pantier, R.,
717 Liggat, K., Mirfazeli, E. S., Hall-Ponsele, E., Mullin, N. P., Wilson, V., & Chambers, I. (2017).
718 Distinct SoxB1 networks are required for naive and primed pluripotency. *Elife*, *6*.
719 https://doi.org/10.7554/eLife.27746
720 Davis, R. L., & Kirschner, M. W. (2000). The fate of cells in the tailbud of Xenopus laevis.
721 *Development*, *127*(2), 255-267. https://doi.org/10.1242/dev.127.2.255

722 Dewari, P. S., Southgate, B., McCarten, K., Monogarov, G., O'Duibhir, E., Quinn, N., Tyrer, A., Leitner,
723 M. C., Plumb, C., Kalantzaki, M., Blin, C., Finch, R., Bressan, R. B., Morrison, G., Jacobi, A. M.,
724 Behlke, M. A., von Kriegsheim, A., Tomlinson, S., Krijgsveld, J., & Pollard, S. M. (2018). An
725 efficient and scalable pipeline for epitope tagging in mammalian stem cells using Cas9
726 ribonucleoprotein. *Elife*, *7*. https://doi.org/10.7554/eLife.35069
727 Edri, S., Hayward, P., Baillie-Johnson, P., Steventon, B. J., & Martinez Arias, A. (2019). An epiblast
728 stem cell-derived multipotent progenitor population for axial extension. *Development*,
729 *146*(10). https://doi.org/10.1242/dev.168187
730 Edri, S., Hayward, P., Jawaid, W., & Arias, A. M. (2019). Neuro-mesodermal progenitors (NMPs): a
731 comparative study between pluripotent stem cells and embryo-derived populations.
732 *Development*, *146*(12). https://doi.org/ARTN dev180190

733 10.1242/dev.180190
734 French, M., Portero, R., Dale, J. K., Blin, G., Wilson, V., & Lowell, S. (2024). A toolkit for mapping cell
735 identities in relation to neighbours reveals Notch-dependent heterogeneity within
736 neuromesodermal progenitor populations. *bioRxiv*, 2024.2009.2003.610492.
737 https://doi.org/10.1101/2024.09.03.610492
738 Gouti, M., Delile, J., Stamataki, D., Wymeersch, F. J., Huang, Y. L., Kleinjung, J., Wilson, V., & Briscoe,
739 J. (2017). A Gene Regulatory Network Balances Neural and Mesoderm Specification during
740 Vertebrate Trunk Development. *Developmental Cell*, *41*(3), 243-+.
741 https://doi.org/10.1016/j.devcel.2017.04.002
742 Gouti, M., Tsakiridis, A., Wymeersch, F. J., Huang, Y. L., Kleinjung, J., Wilson, V., & Briscoe, J. (2014).
743 In Vitro Generation of Neuromesodermal Progenitors Reveals Distinct Roles for Wnt
744 Signalling in the Specification of Spinal Cord and Paraxial Mesoderm Identity. *Plos Biology*,
745 *12*(8). https://doi.org/ARTN e1001937

746 10.1371/journal.pbio.1001937
747 Gruneberg, H. (1958). Genetical studies on the skeleton of the mouse. XXIII. The development of
748 brachyury and anury. *J Embryol Exp Morphol*, *6*(3), 424-443.
749 https://www.ncbi.nlm.nih.gov/pubmed/13575656
750 Guillot, C., Djeffal, Y., Michaut, A., Rabe, B., & Pourquie, O. (2021). Dynamics of primitive streak
751 regression controls the fate of neuromesodermal progenitors in the chicken embryo. *Elife*,
752 *10*. https://doi.org/10.7554/eLife.64819
753 Kinney, B. A., Al Anber, A., Row, R. H., Tseng, Y. J., Weidmann, M. D., Knaut, H., & Martin, B. L.
754 (2020). Sox2 and Canonical Wnt Signaling Interact to Activate a Developmental Checkpoint
755 Coordinating Morphogenesis with Mesoderm Fate Acquisition. *Cell Rep*, *33*(4), 108311.
756 https://doi.org/10.1016/j.celrep.2020.108311
757 Kispert, A., Ortner, H., Cooke, J., & Herrmann, B. G. (1995). The chick Brachyury gene: developmental
758 expression pattern and response to axial induction by localized activin. *Dev Biol*, *168*(2), 406-
759 415. https://doi.org/10.1006/dbio.1995.1090
760 Martin, B. L., & Kimelman, D. (2012). Canonical Wnt signaling dynamically controls multiple stem cell
761 fate decisions during vertebrate body formation. *Dev Cell*, *22*(1), 223-232.
762 https://doi.org/10.1016/j.devcel.2011.11.001
763 Martins-Costa, C., Wilson, V., & Binagui-Casas, A. (2024). Neuromesodermal specification during
764 head-to-tail body axis formation. *Curr Top Dev Biol*, *159*, 232-271.
765 https://doi.org/10.1016/bs.ctdb.2024.02.012
766 Romanos, M., Allio, G., Roussigne, M., Combres, L., Escalas, N., Soula, C., Medevielle, F., Steventon,
767 B., Trescases, A., & Benazeraf, B. (2021). Cell-to-cell heterogeneity in Sox2 and Bra
768 expression guides progenitor motility and destiny. *Elife*, *10*.
769 https://doi.org/10.7554/eLife.66588

770 Row, R. H., Pegg, A., Kinney, B. A., Farr, G. H., Maves, L., Lowell, S., Wilson, V., & Martin, B. L. (2018).
771 BMP and FGF signaling interact to pattern mesoderm by controlling basic helix-loop-helix
772 transcription factor activity. *Elife*, *7*. https://doi.org/ARTN e31018

773 10.7554/eLife.31018
774 Taoudi, S., Morrison, A. M., Inoue, H., Gribi, R., Ure, J., & Medvinsky, A. (2005). Progressive
775 divergence of definitive haematopoietic stem cells from the endothelial compartment does
776 not depend on contact with the foetal liver. *Development*, *132*(18), 4179-4191.
777 https://doi.org/10.1242/dev.01974
778 Tsakiridis, A., & Wilson, V. (2015). Assessing the bipotency of in vitro-derived neuromesodermal
779 progenitors. *F1000Res*, *4*, 100. https://doi.org/10.12688/f1000research.6345.2
780 Tzouanacou, E., Wegener, A., Wymeersch, F. J., Wilson, V., & Nicolas, J. F. (2009). Redefining the
781 Progression of Lineage Segregations during Mammalian Embryogenesis by Clonal Analysis.
782 *Developmental Cell*, *17*(3), 365-376. https://doi.org/10.1016/j.devcel.2009.08.002
783 van den Brink, S. C., Baillie-Johnson, P., Balayo, T., Hadjantonakis, A. K., Nowotschin, S., Turner, D. A.,
784 & Martinez Arias, A. (2014). Symmetry breaking, germ layer specification and axial
785 organisation in aggregates of mouse embryonic stem cells. *Development*, *141*(22), 4231-
786 4242. https://doi.org/10.1242/dev.113001
787 Whittingham, D. G. (1974). Embryo banks in the future of developmental genetics. *Genetics*, *78*(1),
788 395-402. https://doi.org/10.1093/genetics/78.1.395
789 Wilson, V., & Beddington, R. (1997). Expression of T protein in the primitive streak is necessary and
790 sufficient for posterior mesoderm movement and somite differentiation. *Developmental*
791 *Biology*, *192*(1), 45-58. https://doi.org/DOI 10.1006/dbio.1997.8701
792 Wilson, V., Manson, L., Skarnes, W. C., & Beddington, R. S. P. (1995). The T-Gene Is Necessary for
793 Normal Mesodermal Morphogenetic Cell Movements during Gastrulation. *Development*,
794 *121*(3), 877-886. <Go to ISI>://WOS:A1995QN06700023
795 Wymeersch, F. J., Huang, Y. L., Blin, G., Cambray, N., Wilkie, R., Wong, F. C. K., & Wilson, V. (2016).
796 Position-dependent plasticity of distinct progenitor types in the primitive streak. *Elife*, *5*.
797 https://doi.org/ARTN e10042

798 10.7554/eLife.10042
799 Wymeersch, F. J., Wilson, V., & Tsakiridis, A. (2021). Understanding axial progenitor biology in vivo
800 and in vitro. *Development*, *148*(4). https://doi.org/ARTN dev180612

801 10.1242/dev.180612
802 Yamaguchi, T. P., Takada, S., Yoshikawa, Y., Wu, N., & McMahon, A. P. (1999). T (Brachyury) is a
803 direct target of Wnt3a during paraxial mesoderm specification. *Genes Dev*, *13*(24), 3185-
804 3190. https://doi.org/10.1101/gad.13.24.3185

805